Journal of Materials Chemistry A

Accepted Manuscript

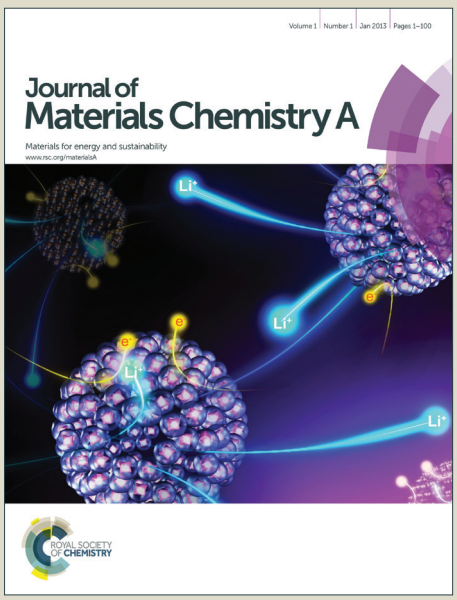

ROYAL SOCIETY OF CHEMISTRY

www.rsc.org/materialsA

Journal Name

ARTICLE

Fullerene C_{70}-TiO_2 Hybrid with Enhanced Photocatalytic Activity under Visible Light Irradiation

Received 00th January 20xx,
Accepted 00th January 20xx

DOI: 10.1039/x0xx00000x

www.rsc.org/

Shengyao Wang,[a, d] Changwei Liu,[a] Ke Dai, *[b] Peng Cai, [b] Hao Chen, *[a, d] Changjun Yang [c] and Qiaoyun Huang [b]

Fullerene C_{70} modified TiO_2 (C_{70}-TiO_2) hybrid was fabricated through a hydrothermal method from titanium sulfate and functionalized C_{70}. The structures of the synthesized hybrids were characterized by X-ray diffraction, UV-vis diffuse reflectance spectroscopy, fourier transform infrared spectroscopy, Raman spectroscopy, scanning electron microscopy, transmission electron microscopy, thermogravimetric analysis, X-ray photoelectron spectroscopy, Brunauer-Emmett-Teller surface area measurement, matrix-assisted laser desorption/ionization-time of flight-mass spectrometer and photoluminescence spectra. The experimental results indicated that the introduction of C_{70} slightly reduces the crystallite size of TiO_2 while extends its adsorption edge to the visible light region. C_{70} molecules were located onto the surface of TiO_2 nanoparticles via covalent bonding, which generated strong interaction between the functionalized C_{70} and TiO_2. The $O_2\bullet^-$, •OH and h^+ are active species which were also proved by trapping experiment. The photocatalytic degradation efficiency of sulfathiazole over C_{70}-TiO_2 hybrid is higher than that over pure TiO_2, C_{60}-TiO_2, and a mechanical mixture of C_{70} and TiO_2 under visible light irradiation. The excellent visible light-induced activity is rationalized by the results of photoluminescence spectra; i.e., the intensity of the emission from C_{70}-TiO_2 hybrid were both found to be weaker than those from pure TiO_2 and C_{60}-TiO_2 hybrid.

Introduction

Recently, the applications in solar energy conversion and degradation of organic pollutants by semiconductor photocatalysts have attracted considerable attention because of their great potential in solving current environment and energy problems with abundant solar light.[1-3] Titanium dioxide (TiO_2) is the most promising semiconductor photocatalytic material because of its excellent physical and chemical properties, such as low cost, long-term stability, strong oxidizing capability, and complete mineralization without generation of toxic byproducts.[4-5] However, the potential for practical application of TiO_2 is restricted by the broad band gap (3.2 eV) and low quantum efficiency. The broad band gap inhibits the absorption of sunlight and the photocatalyst can only be excited under UV irradiation (which is only approximately 4% of solar radiation).[6-7] The photocatalyst can generate photogenerated electrons and holes, which can then migrate to the surfaces and carry out the redox reaction. At the same time, a rapid recombination of the photogenerated electron-hole pairs greatly decreases the efficiency of the photocatalyst and limits its practical application. Therefore, the quantum efficiency of photocatalysis should be enhanced and the band gap of TiO_2 should be decreased to improve the catalytic ability of the photocatalyst for more effective applications. Several attempts have been made to reduce the band gap of TiO_2 and the recombination rate of the photogenerated electron-hole pairs, involving non-metal or metal element doping, coupling with narrow band semiconductors, and dye surface sensitization.[8-12]

TiO_2 modified by carbon dots, such as fullerene, carbon nanotube, and graphene, have received significant attention in the recent years.[13] Carbon dots are highly valued because of their excellent optical performance, small size effect, and ease in achieving surface functionalization towards coupling with TiO_2.[14, 15] As a typical fullerene, C_{60} is an excellent electron acceptor because of its delocalized conjugated structure,[16-17] which can efficiently separate photo-induced charge.[18] To date, numerous studies have focused in studying the combination of C_{60} and other semiconductors, including Bi_2WO_6,[19] $PbMoO_4$,[20] Ag_2S,[21] ZnO,[22] C_3N_4,[23] and TiO_2.[24] Under visible light irradiation, the visible light absorption, the adsorption towards organic composites and morphology of semiconductors could be found have significant effects on acting as an electron reservoir to accept or shuttle photogenerated electrons. Kamat et al.[25] investigated the charge transfer between C_{60} and TiO_2 and found that the migration of the charge from C_{60} to TiO_2 was caused by the two-photo excitation mechanism. Mukther et al.[26] prepared the visible light responsive TiO_2–cyclodextrin–fullerene composite, which showed reduced charge recombination ratio

[a] College of Science, Huazhong Agricultural University, Wuhan 430070, P R China. Email: hchenhao@mail.hzau.edu.cn.
[b] College of Resources and Environment, Huazhong Agricultural University, Wuhan 430070, P R China. Email: dk@mail.hzau.edu.cn.
[c] Key Laboratory of Catalysis and Materials Science of the State South-Central University for Nationalities, Wuhan 430074, P R China.
[d] Key Laboratory of Environment Correlative Dietology, Ministry of Education, Wuhan 430070, P R China.
† Electronic Supplementary Information (ESI) available. See
DOI: 10.1039/x0xx00000x

and enhanced photocatalytic activity. Chai et al.[27] investigated the photocatalytic activity of different carbon loaded TiO_2. When coupled with TiO_2, C_{60}-decorated SWCNTs was more beneficial for the photogenerated carrier separation than SWCNTs and C_{60}. They believed the carbon material possessing a higher electron affinity is necessary when designing a hybrid of carbon and TiO_2 for an enhanced photocatalytic performance.

C_{70} is a close-shell configuration consisting of 35 bonding molecular orbitals with 70 p-electrons which could promote efficient electron transfer reduction.[28] Compared with C_{60}, C_{70} has a higher electron affinity and a higher possibility to form anions or free radicals because of the reduced symmetry structure.[29] In addition, C_{70} has a larger photo cross-sectional area, which suggests that a high harvesting efficiency of light can be expected.[30] Therefore, introduction of C_{70} to TiO_2 may induce excellent visible-light photocatalytic activity. To the best of our knowledge, no prior work regarding the fullerene C_{70}-TiO_2 hybrid photocatalyst has been reported to date.

In the present study, the C_{70}-TiO_2 hybrid was prepared for the first time using the hydrothermal method. The photocatalytic activity of the C_{70}-TiO_2 hybrid was tested and compared with some other analogous photocatalysts by the degradation of sulfathiazole under visible light irradiation. The effect of C_{70} content on the photocatalytic activity of C_{70}-TiO_2 hybrid and the repeatability of the photocatalytic activity were studied in detail. Moreover, the photocatalytic mechanism for C_{70}-TiO_2 hybrid was proposed though the investigations the recombination process of photoinduced electron-hole pairs by the time-resolved photoluminescence decay spectra.

Experimental

Synthsesis of C_{70}-TiO_2 hybrid

C_{70} (purity <99.0 wt%) was purchased from Puyang Yongxin Fullerene Technology Co., Ltd. (CAS, China) and activated as follows: C_{70} was suspended in 35 mL of deionized water and concentrated nitric acid ($v_{(water)}$:$v_{(HNO3)}$ = 7:1), heat stirred for 2h, and then washed with deionized water until the pH value of the supernatant became neutral. Then, the activated C_{70} was collected by centrifugation and dried at 60 °C overnight.

C_{70}-TiO_2 hybrid was prepared using the hydrothermal method. Titanium sulfate, cetyltrimethylammonium bromide (CTAB) and deionized water (m($Ti(SO_4)_2$):m(CTAB):m(water) = 1:0.12:100) were stirred evenly with a certain amount of activated C_{70}. The mixture was transferred to a Teflon lined stainless steel autoclave with 50 mL capacity and heated in oven at 100 °C for 72 h. After cooling to room temperature, the mixture was centrifuged and added with deionized water and ethanol (1:1 v/v). Subsequently, sodium chloride was added to saturation and ion exchange for 24 h, washed with deionized water and ethanol for 2 to 3 times, respectively, and dried at 90 °C for 10 h. Finally, the mixture was calcined at 400 °C for 2 h, and then ground to uniformity.

C_{60}-TiO_2 hybrid was synthesized by the same procedure as above stated. The reference TiO_2 was prepared without the addition of C_{70}. The mechanical mixture of C_{70} and TiO_2 (C_{70}+TiO_2) was obtained by mixed the activated C_{70} and pure TiO_2 in the agate mortar immediately.

Characterization

X-ray diffraction (XRD) patterns were analyzed using an X-ray diffractometer (Bruker Inc., Germany) with Cu Kα radiation source at 35 kV. Raman spectroscopy was conducted using Confocal Raman Microspectroscope (Renishaw Inc., UK). The functional groups formed on the surface of C_{70}-TiO_2 hybrid were examined by Fourier transform infrared (FT-IR) spectroscopy (Nicolet Inc., USA) using the KBr method. The surface state and structure of C_{70}-TiO_2 hybrid were observed by scanning electron microscopy (SEM) (JSM-6700F JEOL, Japan) and transmission electron microscopy (TEM) (JEM-2100F, JEOL, Japan). UV–vis diffused reflectance spectroscopy of the power solids were carried out using a UV–vis spectrophotometer (UV-3100, Shimadzu Inc., Japan). The chemical nature of the interconnection between TiO_2 and C_{70} was tested with an X-ray photoelectron spectrometer (XSAM800, Kratos Analytical Inc., UK). The photoluminescence (PL) spectra were recorded by a fluorescence spectrometer (F-4600, Hitachi Inc., Japan) with 300 nm excitation. Brunauer–Emmett–Teller (BET) surface area was measured by N_2 adsorption-desorption isotherm (ASAP 2020, Micrometrics Inc., USA). Thermogravimetric (TG) analysis was performed in air atmosphere with thermal gravimetric analyzer (TG209, NETZSCH Inc., Germany) under the temperature increased from 30 to 800 °C with a heating rate of 10 °C/min. Matrix-assisted laser desorption/ionization-time of flight-mass (MALDI-TOF-MS) analysis was obtained from MALDI-TOF-MS spectrometer (AXIMA Confidence Shimadzu Inc., Japan) by using dihydroxy-benzoic acid (DHB) as the matrix.

Photocatalytic reactions

The photocatalytic activities of C_{70}-TiO_2 were estimated by degradation of sulfathiazole in aqueous media under visible light and UV light irradiation. A 300 W Xenon lamp (PLS SXE300C, Beijing Perfectlight Inc., China) with a 420 nm cutoff filter was used as the visible light source, with an average light intensity of 600 μW cm^{-2}. An 18 W low−pressure mercury lamp (Guangzhou San Sheng Environmental Protection Technology Co., Ltd., China) were used as radiation sources, with an average light intensity of 14.5 μW cm^{-2}. The experiments were carried out in a photocatalytic reactor with 50 mL aqueous solution of sulfathiazole (10 mg·mL^{-1}) and photocatalyst (1 g·L^{-1}) maintained in a constant temperature through a circulation water jacket.

The suspension containing sulfathiazole and photocatalyst was continuously stirred in the dark for 30 min to establish an adsorption-desorption equilibrium; after which, the xenon lamp was turned on. In our revised manuscript the first sample was collected at the beginning of dark reaction to detect the concentration of sulfathiazole, which was considered as the initial concentration (c_0). The subsequent samples were collected in every 30 min and immediately centrifuged to separate any suspension solid. The clean upper solution was detected using UV–vis spectroscopy to determine the

sulfathiazole concentration (c_t) in different times by measuring its absorbance at 282 nm. Finally, the removal rate was calculated using c_t/c_0.

To detect the active species during photocatalytic reactivity, hydroxyl radicals (•OH), superoxide radical (O_2•$^-$) and holes (h^+) were investigated by adding 1.0 mM IPA (a quencher of •OH), BQ (a quencher of O_2•$^-$) and TEOA (a quencher of h^+), respectively. The method was similar to the former photocatalytic activity test except that the substrate was changed to RhB (10^{-5} mol·L^{-1}), as the sulfathiazole may react with the quencher. The samples were collected after dark reaction and after 60 min irradiation, respectively. The clean upper solution was detected using UV–vis spectroscopy to determine the RhB concentration by measuring its absorbance at 554 nm.

Results and discussion

Morphology, phase structures, and optical properties

The XRD patterns of C_{70}-TiO_2 hybrids with different C_{70} contents are shown in Fig. 1. The peaks at 25.4° (101), 37.5° (004), 48.1° (200), 53.8° (105), 54.8° (211), and 62.8° (204) correspond to the pure anatase phase; the characteristic peaks of rutile and brookite were not detected.[24, 31, 32] The diffraction peaks of anatase phase did not shift with the incorporation of C_{70}, indicating that the addition of C_{70} does not affect the crystalline structure of TiO_2. Even for 24 wt% C_{70}-TiO_2, no diffraction peaks corresponding to C_{70} were observed, which suggests that C_{70} was well-dispersed and interacted with TiO_2 in the hybrid.[33] The average crystal sizes calculated from the broadening of the (101) peaks of anatase were 12.7, 11.7, 11.0, 10.8, 9.3, and 9.2 nm for TiO_2 and 3–24 wt% C_{70}-TiO_2, respectively. The decrease in crystal size indicates that C_{70} prevented the growth of anatase crystal. TiO_2 nanoparticles with small crystal size are beneficial for the transfer of photogenerated carriers from bulk to surface.[34]

The UV-vis diffuse reflectance spectra of TiO_2, C_{70} and C_{70}-TiO_2 hybrids with different C_{70} contents are shown in Fig. 2. the calculated band gap of C_{70}-TiO_2 hybrids with different C_{70} contents indicated that the band gaps were range from 3.17 to 3.22eV (Fig. S1, ESI†), but the hybrids could absorb visible light within a wavelength of longer than 380 nm due to due to the C_{70}-sensitized activation. Meanwhile, significant correlation was observed between the C_{70} content and UV-vis spectrum variation. The absorption of the hybrid catalyst increased with the C_{70} content, indicating that the C_{70}-TiO_2 hybrid can be excited to generate more hole-electron pairs under visible light irradiation. C_{70} has strong absorption in the ultraviolet region and weak but significant bands in the visible region according to the results.[35] Therefore, introducing C_{70} may enhance the photocatalytic activity of TiO_2 under visible light irradiation.[36-38]

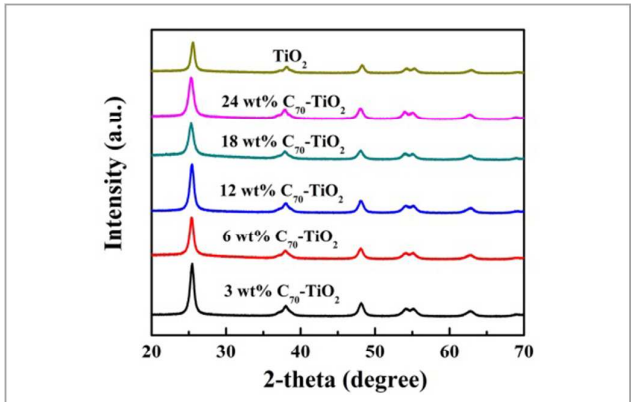

Fig. 1 XRD patterns of TiO_2, C_{70}-TiO_2 with different content of C_{70}.

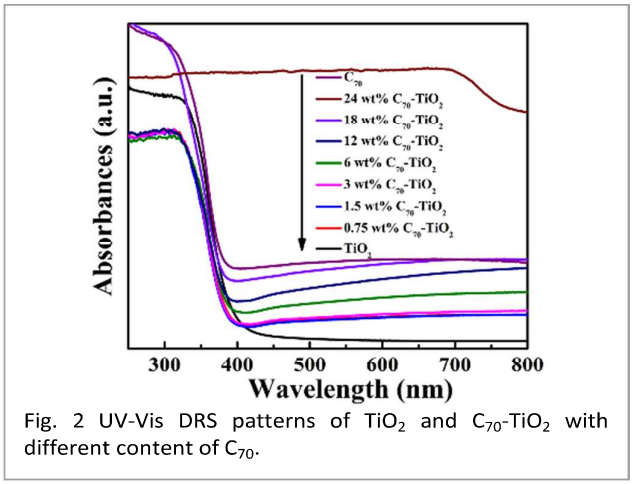

Fig. 2 UV-Vis DRS patterns of TiO_2 and C_{70}-TiO_2 with different content of C_{70}.

The representative SEM and HRTEM images of 18 wt% C_{70}-TiO_2 are displayed in Fig. 3a and 3b. As can be seen from Fig 3a, the surface of hybrid was uneven, which could increase the specific surface area and enhance its photocatalytic activity of TiO_2.[39] TiO_2 nanoparticles were well dispersed and little aggregated. Moreover, TiO_2 nanoparticles had a mean size of ~10nm (Fig. S2, ESI†), but TiO_2 spheres had a homogeneous size in the range from 100 to 192 nm for 18 wt% C_{70}-TiO_2 hybrid, which is related to the presence of well-dispersed C_{70} which inhibited the grain growth of TiO_2 by restricting their direct contact. No presence of C_{70} was identified from the SEM micrograph, because the size of C_{70} was too small to be found at the present magnification scale. Charge migration between C_{70} and TiO_2 was highly related to the interface structure of C_{70}-TiO_2 hybrid. Thus, the morphology of C_{70}-TiO_2 hybrid was further studied by HRTEM. Fig. 3b displays the HRTEM image of the 18 wt% C_{70}-TiO_2. The lattice fringe of sample can be clearly observed and its spacing is measured to be ca. 0.35 nm, which is attributed to the TiO_2 (101) plane.[40] However, the

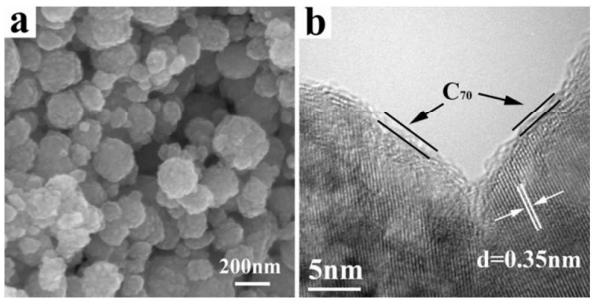

Fig. 3 SEM (a) and TEM (b) images of 18 wt% C_{70}-TiO_2.

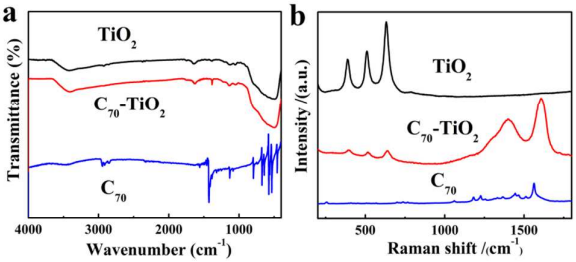

Fig. 4 (a) FT-IR spectra and (b) Raman spectra of TiO_2, C_{70} and C_{70}-TiO_2.

outer boundary of sample was distinctly different. A coverture layer with noncrystal structure surrounded the surface of TiO_2 nanoparticle. The thickness of the coverture layer was estimated to be about 1 nm, which was close to the diameter of C_{70} molecule. Thus, it can be estimated that the outer layer was C_{70} that dispersed on the surface of TiO_2 with a monolayer structure.[41]

IR and Raman spectra

Fig. 4a displays the FT-IR spectra of C_{70}, TiO_2, and C_{70}-TiO_2 hybrid. The bands at 456, 534, 563, 576, 640, 673, 794, 1132, and 1429 cm^{-1} are attributed to the internal modes of the C_{70} molecule.[42-44] In the region of 400 cm^{-1} to 1000cm^{-1}, the spectra of C_{70}-TiO_2 showed no characteristic absorption peak of C_{70} due to the strong absorption for anatase in the region. The characteristic absorption peaks at 1132 and 1429 cm^{-1} in the spectra for C_{70}-TiO_2 were quite weak, indicating that C_{70} was well-dispersed in the TiO_2, which is in accord with the XRD results. In addition, the structure of anatase was not changed after the introduction of C_{70}. However, the stretching vibrations of the Ti-O-Ti bonds (502 cm^{-1}) slightly red-shifted to low frequency, which may be associated with the formation of covalent bonds (Ti-O-C=O or Ti-O-C) after C_{70}'s introduction.[31]

Fig. 4b shows the Raman spectra of TiO_2, C_{70}, and C_{70}-TiO_2 hybrid. The vibration peaks at 399 cm^{-1} (B_{1g}), 517 cm^{-1} (A_{1g}), and 638 cm^{-1} (E_g) are present in the spectra, suggesting that the TiO_2 nanoparticles exhibited the anatase phase for pure TiO_2 and C_{70}-TiO_2 hybrid.[45] Compared with pure TiO_2, the characteristic absorption peaks of the anatase in the C_{70}-TiO_2 spectra were broader and the intensity of the peaks were weaker, indicating introduced C_{70} inhibited the growth of TiO_2 grains and generated more defect sites on the TiO_2 surface. The peaks at 1060, 1182, 1226, 1443, 1511, and 1564 cm^{-1} were the characteristic absorption peaks of C_{70}.[46] These peaks were absent in the C_{70}-TiO_2 spectrum, which imply that the symmetric vibrations of C_{70} molecules were restricted due to the formed covalent bonds between C_{70} and TiO_2. However, internal vibrations of C_{70} at 1401 and 1608 cm^{-1}, which stand for the disordered carbon (D-line) and graphite carbon (G-line), can still be observed. The I_D/I_G (the ratio of the intensity of peaks for D-line and G-line) for C_{70}-TiO_2 hybrid was calculated to be 0.55, indicating that the graphitization structure was still the major part.[47, 48] This result confirmed that the original structure of C_{70} was not destroyed after the functionalization in nitric acid or the hydrothermal treatment.

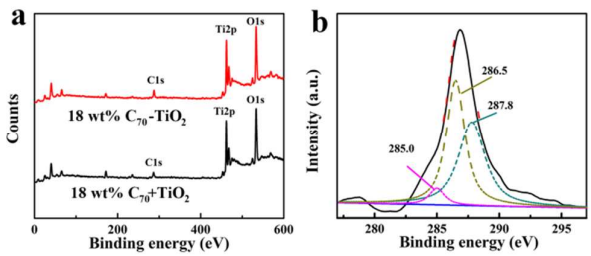

Fig. 5 (a) XPS survey of 18 wt% C_{70}-TiO_2 and 18 wt% C_{70}+TiO_2 and (b) high-resolution C 1s spectra of 18 wt% C_{70}-TiO_2.

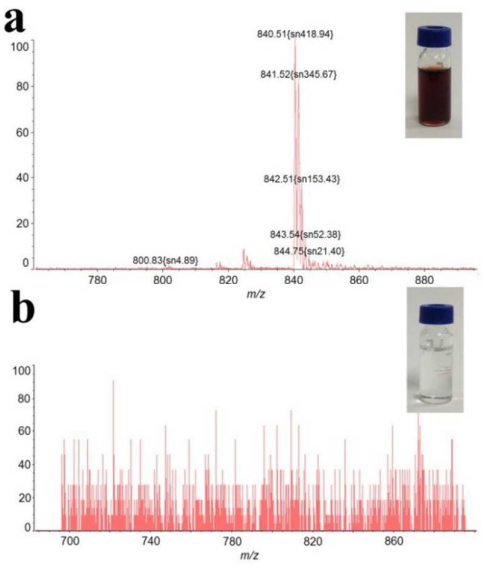

Fig. 6 MALDI-TOF-MS spectra of 18 wt% C_{70}+TiO_2 (a) and

Chemical composition, BET surface areas, and pore size distributions

The real content of C_{70} in the C_{70}-TiO_2 hybrids could be determined by TG analysis. TG curves of different contents of C_{70}-TiO_2 was obtained under air atmosphere (Fig. S3, ESI†). As can be seen, C_{70} only decomposes over 500 °C, the weight loss below 500 °C should be assigned to the free water loss and the decomposition of functional groups (Fig. S3a, ESI†). The TG curve of 18 wt% C_{70}-TiO_2 hybrid displays an obvious inflection point compared with the TiO_2 around 500 °C, which comes from the weight loss caused by C_{70} oxidation. According to this, the C_{70} weight ratios in the C_{70}-TiO_2 hybrids were calculated to be 0.6, 1.3, 2.8, 4.9, 6.4, 8.5 and 10.3 wt% for 0.75, 1.5, 3, 6, 12, 18 and 24 wt% C_{70}-TiO_2 hybrids, respectively (Fig. S3b, ESI†). The difference between the calculated values by TG analysis and the estimated values of C_{70} content mainly comes from the loss of unbounded C_{70}, which can be easily washed away with deionized water and ethanol during the preparation of C_{70}-TiO_2 hybrid.

XPS measurements were performed to evaluate the interaction of TiO_2 and C_{70} (Fig. 5). The XPS survey spectra of 18 wt% C_{70}-TiO_2 and 18 wt% C_{70}+TiO_2 (a mechanical mixture of TiO_2 and C_{70}) are shown in Fig. 5a. Compared with C_{70}+TiO_2, the binding energy of C 1s and O 1s of C_{70}-TiO_2 shifted to the

higher region, implying that the addition of C_{70} influenced the chemical nature of the interconnection of TiO_2 and C_{70}. Fig. 5b displays the XPS spectra of the C 1s region of the 18 wt% C_{70}-TiO_2 hybrid, which indicates the coexistence of various chemical bonds. According to the Gaussian curve fitting, the C 1s binding energies are located at about 285.0, 286.5, and 287.8 eV. The main C 1s peak at 287.8 eV was attributed to the carbonyl carbon. The sharp peak at 286.5 eV was assigned to the oxidized species C-O caused by the oxidation of defective sp^2-hybridized carbon in C_{70}. A weak peak was also observed at 285.0 eV, which was contributed by the sp^2-hybridized carbon from C_{70}. These surface functional groups were also verified in Meng's research,[35] which demonstrated that carbonylic functional groups generated on the surface of C_{60} after oxidation treatment by the combination of C_{60} and CoS_2 particles. The C=O and C-O bonds in C_{70}-TiO_2 hybrid imply the formation of covalent bonds between TiO_2 and C_{70}.

To further confirm the chemical bonds between C_{70} and TiO_2 in the hybrid, matrix-assisted laser desorption/ionization-time of flight-mass (MALDI-TOF-MS) spectrometry was employed to analysis C_{70}-TiO_2 hybrid and C_{70}+TiO_2 mixture. 18 wt% C_{70}-TiO_2 hybrid and 18 wt% C_{70}+TiO_2 (a mechanical mixture) were firstly dispersed in toluene and then the solid was removed by centrifuge, respectively. It can be observed that the supernate obtained from the mechanical mixture sample is brown (inset, Fig. 6a) but that from the hybrid is colorless (inset, Fig. 6b). These phenomena indicates that C_{70} in the C_{70}+TiO_2 mixture dissolve easily in toluene whereas C_{70} in the C_{70}-TiO_2 hybrid do not dissolve due to the covalent bonds formed between C_{70} and TiO_2 in the hybrid. In addition, the molecular weight peak (840 m/z) of C_{70} was found in the MALDI-TOF-MS spectrum of C_{70}+TiO_2 mixture, as shown in Fig. 6a. However, no molecular ion peak of C_{70} can be observed in Fig. 6b. These experimental results confirm the formation of covalent bonds between TiO_2 and C_{70}, which is in accordance with the FT-IR and XPS results.

The porous structure and BET surface area of C_{70}-TiO_2 was measured by using nitrogen adsorption–desorption. The BET surface area for the 18 wt% C_{70}-TiO_2 was measured to be 86.24 m^2/g. High specific surface area of C_{70}-TiO_2 hybrid can provide strong adsorption capacity, which would promote its photocatalytic efficiency.[49] Fig. 7 shows the nitrogen adsorption–desorption isotherms and pore size distribution for 18 wt% C_{70}-TiO_2. C_{70}-TiO_2 hybrid showed a type IV curve with a typical hysteresis loop associated with capillary condensation of gases within mesopores, indicating that the catalyst has a mesoporous structure.[50] The pore size distribution (inset of Fig. 7) showed a bimodal pore-size distribution consisting of a small size (3.4 nm) for the intraparticle pores and larger (12.5 nm) interparticle pores. Compared with pure TiO_2,[51] interparticle pore size of C_{70}-TiO_2 hybrid is smaller. This phenomenon revealed the close-packed structure between TiO_2 nanoparticles and C_{70}.

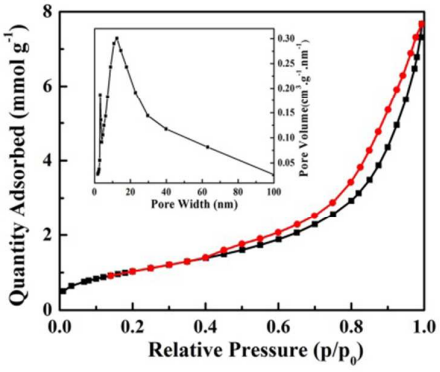

Fig. 7 Nitrogen adsorption–desorption isotherm and pore size distributions (inset) for 18 wt% C_{70}-TiO_2.

Photocatalytic activity of C_{70}-TiO_2 hybrid

Sulfathiazole is a classic synthetic antibiotic in the group of sulfonamides drugs. Contrary to dye, it does not absorb visible light nor have sensitization effect. Therefore, to exclude the photosensitization effect, sulfathiazole was used as the substrate to test the photocatalytic activity of C_{70}-TiO_2 hybrid under different light resources irradiation. Fig. 8a and 8b shows the removal rate of sulfathiazole upon C_{70}-TiO_2 hybrid photocatalyst with different C_{70} content. Under visible light irradiation, no obvious enhancement was observed on the photocatalytic activity of C_{70}-TiO_2 until C_{70} content enhanced to 6 wt% (Fig. 8a). After that, the photocatalytic activity increases firstly and then decreases slightly with further increase on C_{70} content. The best photocatalytic activity is achieved at 18 wt% C_{70}-TiO_2. The results showed that the added C_{70} greatly affected the photocatalytic activity of the hybrid. For C_{70}-TiO_2 with C_{70} content less than 6 wt%, C_{70} was mainly embedded inside by TiO_2 nanoparticles. As a result, little C_{70} can be irradiated and excited by the visible light, and thus no visible-light-induced photoactivity was observed.[52] Although abundant C_{70} is propitious to effectively utilize visible light and generate large numbers of electrons, excessive C_{70} can aggregate to form clusters on the surface of C_{70}-TiO_2, which may hinder the photocatalyst to absorb the visible light, thereby inhibiting the photocatalytic activity. In a word, these phenomena can be explained by the balance between the increase in the synergistic effect from higher C_{70} loadings and the insufficient amounts of TiO_2 and/or blockage of TiO_2 active sites.

Contrary to the results under visible light irradiation, the photocatalytic activity of C_{70}-TiO_2 hybrid is almost unchanged upon varying C_{70} loadings under UV light irradiation (Fig. 8b). It

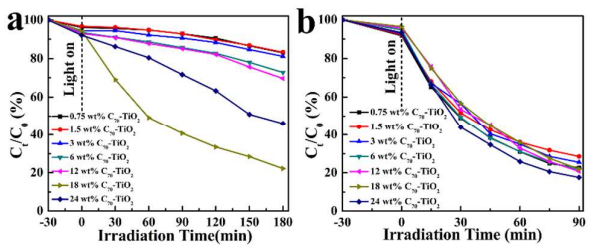

Fig. 8 Photocatalytic degradation efficiencies of sulfathiazole over C_{70}-TiO_2 hybrid with different content of the C_{70} under visible light (a) and UV light (b).

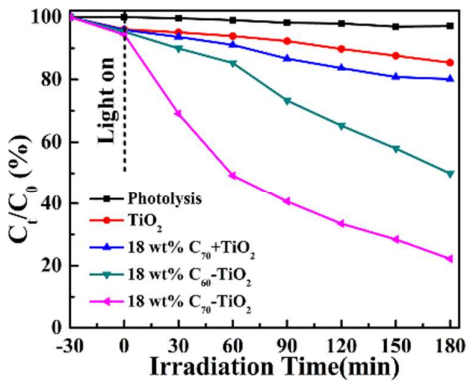

Fig. 9 Photocatalytic degradation efficiencies of sulfathiazole over different photocatalyst under visible light irradiation.

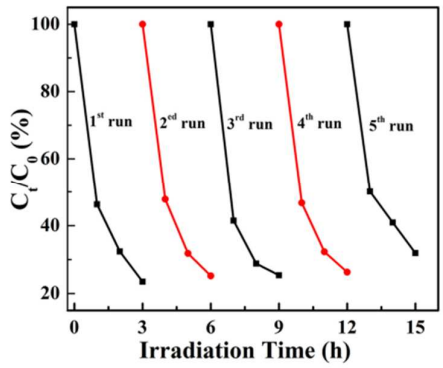

Fig. 10 Cycled experiment on photocatalytic degradation of sulfathiazole over 18 wt% C_{70}-TiO_2 under visible light irradiation.

is worthy noted that 0.75 wt% C_{70}-TiO_2 possessed equivalent photocatalytic activity to 18 wt% C_{70}-TiO_2. Under UV light irradiation, TiO_2 nanoparticles rather than C_{70} contribute most to the UV light adsorption and electrons' generation. Due to its good dispersion, small amount of C_{70} (0.75 wt%) can effectively increase the photocatalytic activity of TiO_2. Although C_{70} additive can benefits the transfer of electrons and inhibit the recombination of excitons, excessive C_{70} can aggregate to form clusters and prevent TiO_2 from absorbing UV light.

The removal rates of sulfathiazole over TiO_2, C_{70}+TiO_2 mixture, C_{70}-TiO_2 hybrid, and C_{60}-TiO_2 hybrid are shown in Fig. 9. As can be seen, in the absence of photocatalyst, the removal rate of sulfathiazole was less than 3% after 3 hours' irradiation, suggesting that the photolysis of sulfathiazole could be neglected. In addition, bare functionalized C_{70} showed no activity for the photocatalytic degradation of sulfathiazole under our experimental conditions. As expected, pure TiO_2 showed inefficient photocatalytic activity because the light absorption edge of TiO_2 is about 400 nm.[51] C_{70}+TiO_2 mixture demonstrated the similar photoactivity to that of pure TiO_2. It should be underlined that C_{70}-TiO_2 hybrid exhibited the best photocatalytic activity among the photocatalysts tested, which

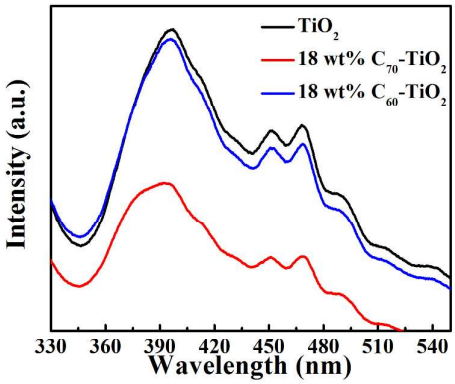

Fig. 11 PL spectra for TiO_2, 18 wt% C_{60}-TiO_2, and 18 wt% C_{70}-TiO_2.

is about 4.2 times higher than that of C_{70}+TiO_2 mixture. These phenomena indicated that the loose contact between C_{70} and TiO_2 in the mechanical mixture would not lead to an efficient visible light activity because visible-light-induced electrons cannot be effectively transferred. In other word, effective combination of C_{70} and TiO_2 is a crucial factor for the visible-light-induced photoactivity of C_{70}-TiO_2 hybrid. Long et al. showed the photocatalytic activity of TiO_2 nanorods obviously enhanced when C_{60} was incorporated into the TiO_2 nanorods due to the effective combination of C_{60} and TiO_2.[41] The incorporated C_{60} facilitated the separation of photoinduced electron-hole pairs and served as the active site to form the active oxygen species.

Herein, we compared the photoactivity of C_{60}-TiO_2 hybrid and C_{70}-TiO_2 hybrid towards sulfathiazole degradation. As shown in Fig. 9, the photocatalytic activity of C_{70}-TiO_2 hybrid is 1.6 times as high as that of C_{60}-TiO_2 hybrid. There are two main reasons accounting for the efficient photocatalytic activity of C_{70}-TiO_2 hybrid. One is the larger photo cross-sectional area of C_{70} molecule, which leads to a high efficiency harvesting of incident light for C_{70}-TiO_2 hybrid. The other is the bigger delocalization effect and higher electron affinity of C_{70} molecule, which benefits the transfer of electrons and facilitates the separation of photogenerated electron–hole pairs. [53] It can be seen from Fig. 8 and 9 that the difference of adsorption among TiO_2, other different photocatalyst and C_{70}-TiO_2 hybrids with different C_{70} contents were not significant. The higher degradation rate mainly resulted from the higher photocatalytic activity of the catalyst.

Long-term stability is an important feature for the photocatalyst in practical application. To study the stability of C_{70}-TiO_2 hybrid, the photocatalyst was collected after photocatalytic reaction, and then dried for the subsequent photocatalytic reaction under identical experimental conditions. The results of the five cycle tests are shown in Fig. 10. After five consecutive runs of 15 hours' accumulative irradiation, the removal rate of sulfathiazole seldom decreased and can still reach 90% of first run, indicating the excellent stability of photocatalytic activity of C_{70}-TiO_2 hybrid.

Mechanism of the enhanced photoreactivity of C_{70}-TiO_2 hybrid

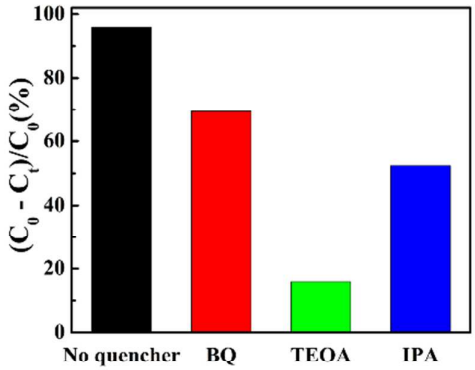

Fig. 12 Trapping experiment of active species during the photocatalytic reaction with 60 min Xenon lamp irradiation (λ ≥ 420 nm)

The photocatalytic activity of semiconductor is closely related to the separation efficiency of photogenerated electrons and holes. Photoluminescence (PL) emission mainly results from the recombination of excited electrons and holes, and lower PL intensity normally indicates higher separation efficiency.[54] The photogenerated carrier separation efficiency for the 18 wt% C_{70}-TiO_2 was estimated by PL spectra. Fig. 11 shows the PL spectra for TiO_2, 18 wt% C_{60}-TiO_2, and 18 wt% C_{70}-TiO_2. The results showed that the fluorescence intensity for C_{70}-TiO_2 was weaker than the pure TiO_2 and C_{60}-TiO_2, indicating that the introduction of C_{70} can inhibit the recombination of photogenerated electron-hole pairs and enhance the photocatalytic activity.[55-57] Thus, more electrons and holes can participate in the photocatalytic reaction. Therefore, the photocatalytic efficiency for the 18 wt% C_{70}-TiO_2 would be higher than the pure TiO_2 and 18 wt% C_{60}-TiO_2, which was confirmed in the photocatalytic degradation of sulfathiazole.

Fig. 12 shows the trapping experiment of active species. It can be seen that the photocatalytic degradation of RhB all decreases with the addition of BQ, IPA and TEOA. Therefore, it can be concluded that $O_2\bullet^-$, •OH and h^+ are all present as the active species. In addition, with the addition of TEOA (a quencher of h^+) photocatalytic degradation of RhB decreases obviously. The reason is that •OH cannot be generated smoothly as the h^+ are trapped.

Based on the above results and discussion, the possible photocatalytic mechanism for C_{70}-TiO_2 hybrid was proposed and shown in Fig. 13. Under UV light irradiation (Fig. 13a), the electrons on the valence band of TiO_2 were excited to the conduction band. The conduction band position of TiO_2 is more negative than C_{70}/C_{70}^-. The former one has a potential of −0.5 V (vs. NHE) while the latter one is −0.2 V (vs. NHE).[38] Due to the intimate contact between C_{70} and TiO_2 in the hybrid, the electrons on the conduction band of TiO_2 were allowed to transfer to C_{70}.[46, 57] Meanwhile, C_{70} was excited from the ground state to a transient state ($^1C_{70}^*$), and then went through a rapid intersystem crossing to a lower lying triplet state ($^3C_{70}^*$).[58, 59] Therefore, the transference of electrons among $^1C_{70}^*$, $^3C_{70}^*$ and ground state of C_{70} could reduce the probability of electrons fall down to the conduction band of TiO_2 and inhibit the recombination of the electrons and holes, which eventually enhance the photocatalytic activity of C_{70}-TiO_2 hybrid.

When the light source was changed into visible light (Fig. 13b), the mechanism of C_{70}-TiO_2 was different as the electrons on the valence band of TiO_2 cannot be excited to the conduction band of TiO_2. While the band gap energy of C_{70} is about 1.9 eV, the visible region of C_{70} is a week but significant bands.[60, 61] Under the visible light irradiation, the electrons can be excited smoothly both from the valence band of TiO_2 to the mid-gap band and from mid-gap band to the conduction band of TiO_2, as a result of the produced mid-gap band of TiO_2 and the chemical bonds between two combinations. Owing to the mid-gap band, visible light can be effectively utilized by the C_{70}-TiO_2 hybrid and turned into photogenerated electrons and holes more efficiently. Meanwhile, the electrons transmitted to the conduction band of TiO_2 was allowed to react with the dissolved O_2, and the water could be also oxidized by the holes on the surface of hybrid then generating more hydroxyl radicals (•OH) and superoxide ions ($\bullet O_2^-$). Both $\bullet O_2^-$ and •OH are considered as radical species in the photocatalysis which would enhanced reaction of sulfathiazole degradation in the solution under the visible light irradiation.

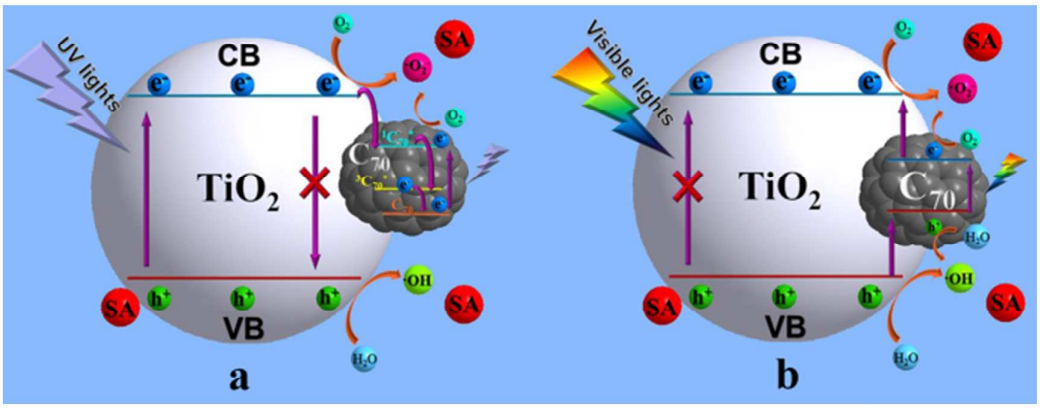

Fig. 13 Photoreaction mechanism of C_{70}-TiO_2 hybrid under UV light irradiation (a) and visible light irradiation (b).

Conclusions

In summary, C_{70}-TiO_2 hybrid with enhanced photocatalytic activity was prepared by a hydrothermal method firstly and characterized by XRD, DRS, FT-IR, Raman, SEM, TEM, TG, XPS, BET, MALDI-TOF-MS, and PL. It was found that introduced C_{70} formed a monolayer onto TiO_2 nanoparticles by covalent bonding, which slightly reduces the crystallite size of TiO_2 while extends its adsorption edge to the visible light region. Under UV/Visible light irradiation, the photocatalytic activity of C_{70}-TiO_2 hybrid was investigated by the degradation of sulfathiazole. The enhanced visible-light-driven photocatalytic performance of C_{70}-TiO_2 was attributed to the inhibited recombination of photogenerated charge carriers and efficient visible light adsorption, which come from the strong electron affinity and large photo cross-sectional area, respectively. Moreover, the $O_2\bullet^-$, •OH and h^+ are active species which were also proved by trapping experiment. The C_{70}-TiO_2 hybrid showed a stable photocatalytic activity in five recycling runs of the degradation experiment.

Acknowledgements

The research was financially supported by the National Natural Science Foundation of China (21307035, 51572101), Natural Science Foundation of Hubei Province (2014CFB919), Fundamental Research Funds for the Central Universities of China (2013PY112), South-Central University for Nationalities (CZY14003) and Open Foundation of Key Laboratory of Catalysis and Materials Science of the State Ethnic Affairs Commission and Ministry of Education, South-Central University for Nationalities (CHCL12004).

Notes and references

1. X. Han, Q. Kuang, M. Jin, Z. Xie and L. Zheng, *J. Am .Chem. Soc.*, 2009, **131**, 3152-3153.
2. A. Mills, R. H. Davies and D. Worsley, *Chem. Soc. Rev.*, 1993, **22**, 417-425.
3. A. L. Kaledin, T. Lian, C. L. Hill and D. G. Musaev, *J. Phys. Chem. C.*, 2012, **116**, 20937-20948.
4. K. Sunada, Y. Kikuchi, K. Hashimoto and A. Fujishima, *Environ. Sci. Technol.*, 1998, **32**, 726-728.
5. S. Wang, L. Zhao, L. Bai, J. Yan, Q. Jiang and J. Lian, *J. Mater. Chem. A.*, 2014, **2**, 7439-7445.
6. N. D. Petkovich, S. G. Rudisill, B. E. Wilson, A. Mukherjee and A. Stein, *Inorg. Chem.*, 2014, **53**, 1100-1112.
7. M. D. Alonso, F. Fresno, S. Suarez and J. M. Coronado, *Energ. Environ. Sci.*, 2009, **2**, 1231-1257.
8. P. N. Kumar, R. Narayanan, M. Deepa and A. K. Srivastava, *J. Mater. Chem. A.*, 2014, **2**, 9771-9783.
9 Z. Xiong and X. S. Zhao, *J. Am. Chem. Soc.*, 2012, **134**, 5754-5757.
10. X. Pan, M. Q. Yang, X. Fu, N. Zhang and Y. J. Xu, *Nanoscale*, 2013, **5**, 3601-3614.
11. A. Bumajdad and M. Madkour, *Phys. Chem. Chem. Phys.*, 2014, **16**, 7146-7158.
12. S. Bingham and W. A. Daoud, *J. Mater. Chem.*, 2011, **21**, 2041-2050.
13. G. Li, B. Jiang, X. Li, Z. Lian, S. Xiao, J. Zhu, D. Zhang and H. Li, *ACS. Appl. Mater. Interfaces*, 2013, **5**, 7190-7197.
14. P. Piotrowski, J. Pawowska, J. Pawowski, A. Wickowska, R. Bilewicz and A. Kaim, *J. Mater. Chem. A.*, 2014, **2**, 2353.
15. Z. Y. Yang, Y. Yao, L. He, Y. Zhong, Y. Ma and J. Yao, *J. Mater. Chem. A.*, 2015, **3**, 10060-10068.
16. M. Q. Yang, N. Zhang and Y. J. Xu, *ACS. Appl. Mater. Interfaces*, 2013, **5**, 1156-1164.
17. W. Bai, V. Krishna, J. Wang, B. Moudgil and B. Koopman, *Appl. Catal. B.*, 2012, **125**, 128-135.
18. C. Sanchez, V. Lanzilotto, C. Gonzalez, A. Verdini, P. L. de Andres, L. Floreano, M. F. Lopez and J. A. MartinGago, *Chem. Eur. J.*, 2012, **18**, 7382-7387.
19. X. Zhao, H. Liu, Y. Shen and J. Qu, *Appl. Catal. B.*, 2011, **106**, 63-68.
20. K. Dai, Y. Yao, H. Liu, I. Mohamed, H. Chen and Q. Huang, *J. Mole. Catal. A.*, 2013, **374–375**, 111-117.
21. Z. D. Meng, T. Ghosh, L. Zhu, J. G. Choi, C. Y. Park and W. C. Oh, *J. Mater. Chem.*, 2012, **22**, 16127.
22. H. Fu, T. Xu, S. Zhu and Y. Zhu, *Environ. Sci. Technol.*, 2008, **42**, 8064-8069.
23. B. Chai, X. Liao, F. Song and H. Zhou, *Dalton. Trans.*, 2014, **43**, 982-989.
24. K. Dai, T. Peng, D. Ke and B. Wei, *Nanotechnology*, 2009, **20**, 125603.
25. P. V. Kamat, M. Gevaert and K. Vinodgopal, *J. Phys. Chem. B.*, 1997, **101**, 4422-4427.
26. M. Mukthar Ali and K. Y. Sandhya, *Carbon*, 2014, **70**, 249-257.
27. B. Chai, T. Peng, X. Zhang, J. Mao, K. Li and X. Zhang, *Dalton. Trans.*, 2013, **42**, 3402-3409.
28. G. E. Scuseria, *Chem. Phys. Lett.*, 1991, **180**, 451-456.
29. J. W. Arbogast and C. S. Foote, *J. Am. Chem. Soc.*, 1991, **113**, 8886-8889.
30. Y. He, J. You, L. Dou, C. C. Chen, E. Richard, K. C. Cha, Y. Wu, G. Li and Y. Yang, *Chem. Commun.*, 2012, **48**, 7616-7618.
31. J. Yu, T. Ma, G. Liu and B. Cheng, *Dalton. trans.*, 2011, **40**, 6635.
32. Z. D. Meng, L. Zhu, J. G. Choi, M. L. Chen and W. C. Oh, *J. Mater. Chem.*, 2011, **21**, 7596.
33. B. Gao, G. Z. Chen and G. Li Puma, *Appl. Catal. B.*, 2009, **89**, 503-509.
34. Q. Xiang, K. Lv and J. Yu, *Appl. Catal. B.*, 2010, **96**, 557-564.
35. Z. D. Meng, L. Zhu, K. Ullah, S. Ye, Q. Sun, W. K. Jang and W. C. Oh, *Mater Res Bull.*, 2014, **49**, 272-278.
36. L. Zhang, Y. Wang, T. Xu, S. Zhu and Y. Zhu, *J. Mole. Catal. A.*, 2010, **331**, 7-14.
37. Y. Yang, Y. Yao, L. He, Y. Zhong, Y. Ma and J. Yao, *J. Mater. Chem. A.*, 2015, **3**, 10060-10068.
38. Y. Hu, X. Gao, L. Yu, Y. Wang, J. Ning, S. Xu and X. W. Lou, *Angew. Chem. Int. Edit.*, 2013, **52**, 5636-5639.
39. A. O. Ibhadon, G. M. Greenway, Y. Yue, P. Falaras and D. Tsoukleris, *Appl. Catal. B.*, 2008, **84**, 351-355.
40. Y. Long, Y. Lu, Y. Huang, Y. Peng, Y. Lu, S.-Z. Kang and J. Mu, *J. Phys. Chem. C.*, 2009, **113**, 13899-13905.

41. J. Yu, W. Wang, B. Cheng and B. L. Su, *J. Phys. Chem. C.*, 2009, **113**, 6743-6750.
42. D. M. Cox, S. Behal, M. Disko, S. M. Gorun, M. Greaney, C. S. Hsu, E. B. Kollin, J. Millar and J. Robbins, *J. Am. Chem Soc.*, 1991, **113**, 2940-2944.
43. G. Klupp, F. Borondics, Z. Gillay, K. Kamaras and L. Forro, *Ferroelectrics.*, 2001, **249**, 117-124.
44. V. Schettino, M. Pagliai and G. Cardini, *J. Phys. Chem. A.*, 2002, **106**, 1815-1823.
45. P. Falaras, A. Hugot Le Goff, M. C. Bernard and A. Xagas, *Sol. Energ. Mater. Sol. C.*, 2000, **64**, 167-184.
46. D. S. Bethune, G. Meijer, W. C. Tang and H. J. Rosen, *Chem. Phys. Lett.*, 1990, **174**, 219-222.
47. C. M. Chen, Y. M. Dai, J. G. Huang and J, M, Jehng, *Carbon*, 2006, **44**, 1808-1820.
48. S. M. Miranda, G. E. Romanos, V. Likodimos, R. R. N. Marques, E. P. Favvas, F. K. Katsaros, K. L. Stefanopoulos, V. J. P. Vilar, J. L. Faria, P. Falaras and A. M. T. Silva, *Appl. Catal. B.*, 2014, 147, 65-81.
49. Q. Xiang, J. Yu and M. Jaroniec, *Nanoscale*, 2011, **3**, 3670-3678.
50. K. M. S. Khalil, *J. Colloid. Interf. Sci.*, 2007, **307**, 172-180.
51. T. Peng, D. Zhao, K. Dai, W. Shi and K. Hirao, *J. Phys. Chem. B.*, 2005, **109**, 4947-4952.
52. S. K. Mohapatra, N. Kondamudi, S. Banerjee and M. Misra, *Langmuir*, 2008, **24**, 11276-11281.
53. A. Di Paola, E. Garcia Lopez, G. Marci and L. Palmisano, *J. Hazard. Mater.*, 2012, **211-212**, 3-29.
54. L. Ye, L. Zan, L. Tian, T. Peng and J. Zhang, *Chem. Commun.*, 2011, **47**, 6951-6953.
55. V. Subramanian, E. E. Wolf and P. V. Kamat, *J. Am. Chem. Soc.*, 2004, **126**, 4943-4950.
56. D. Wang, L. Guo, Y. Zhen, L. Yue, G. Xue and F. Fu, *J. Mater. Chem. A.*, 2014, **2**, 11716-11727.
57. Z. Lian, P. Xu, W. Wang, D. Zhang, S. Xiao, X. Li and G. Li, *ACS. Appl. Mater. Interfaces*, 2015, **7**, 4533-4540.
58. P. M. Allemand, A. Koch, F. Wudl, Y. Rubin, F. Diederich, M. M. Alvarez, S. J. Anz and R. L. Whetten, *J. Am. Chem. Soc.*, 1991, **113**, 1050-1051.
59. N. Tezuka, T. Umeyama, S. Seki, Y. Matano, M. Nishi, K. Hirao and H. Imahori, *J. Phys. Chem. C.*, 2010, **114**, 3235-3247.
60. R. Singhal, F. Singh, A. Tripathi and D. K. Avasthi, *Radiat. Eff. Defect. S.*, 2009, **164**, 38-48.
61. M. Ichida, S. Tanaka and A. Nakamura, *Solid. State. Commun.*, 2000, **116**, 615-619.

Colour graphic

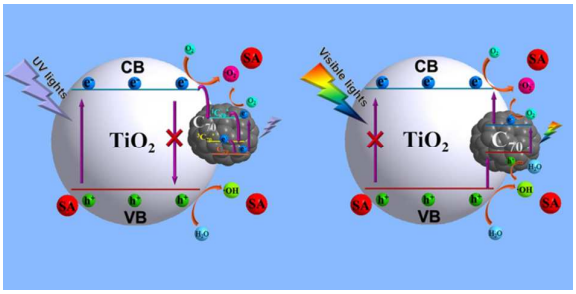

Longer-lived photo-generated charge carriers and efficient visible light adsorption give birth to the excellent visible-light-driven photoactivity of C_{70}-TiO_2 hybrid.